PHILOSOPHICAL TRANSACTIONS OF THE ROYAL SOCIETY A MATHEMATICAL, PHYSICAL & ENGINEERING SCIENCES

A High Resolution Solar Ultraviolet Spectrum between 200 and 220 nm

B. C. Boland, B. B. Jones, R. Wilson, S. F. T. Engstrom and G. Noci

Phil. Trans. R. Soc. Lond. A 1971 **270**, 29-46
doi: 10.1098/rsta.1971.0057

Phil. Trans. Roy. Soc. Lond. A. **270**, 29–46 (1971) [29]
Printed in Great Britain

A high resolution solar ultraviolet spectrum between 200 and 220 nm

By B. C. Boland, B. B. Jones, R. Wilson
Astrophysics Research Unit, Culham, Berkshire

S. F. T. Engstrom
Stockholm Observatory, Sweden

and G. Noci
Osservatorio Astrofisico di Arcetri, Florence, Italy

[Plates 1 and 2]

A high resolution solar spectrum in the range 200 to 220 nm has been recorded with an echelle spectrograph launched in a sun-pointing Skylark rocket. The data have been reduced and are presented as intensity–wavelength plots together with a wavelength list and proposed identifications.

A broad absorption feature at 212.4 nm is assigned to a single source and an intensity analysis confirms this to be the non-resonance Si I line at 212.412 nm.

The discontinuity in the continuum intensity near 208.7 nm is revealed with high resolution for the first time and is assigned to the photoionization edge of Al I. An analysis shows that its intensity drop and wavelength position can only be explained by adjustments to the solar model in the region

$$0.001 < T_{5000} < 0.2.$$

Introduction

A high resolution spectrum of the solar disk in the wavelength range $\lambda 200$ to $\lambda 220$ nm was recorded photographically during a flight of a sunpointing Skylark rocket launched from Woomera at 04 h 21 min U.T. on 22 April 1969. The payload reached an apogee of 178 km and during the flight four exposures of 10, 25, 100 and 50 s were made in that order, starting at a height of 130 km and continuing through apogee to 140 km on the descent. Solar spectra were obtained on each exposure, the longest one having a background fog density between D 0.1 and D 0.2. The in-flight spectral resolution was 3 pm.

The data have been reduced and are presented graphically as intensity–wavelength plots together with a wavelength list giving 663 absorption lines with proposed identifications for nearly 90 %.

Some apparently broad absorption features are revealed in the spectrum. Although many of these are due to line clumping, at least one (at 212.4 nm) is due to a single broad absorption line which is crossed by a number of sharp lines. The discontinuity in the continuum intensity near 208.7 nm is shown at high resolution for the first time and its structure and production have been investigated.

Instrumentation

The layout of the optical system is given in figure 1. The spectrograph uses reflecting optical components incorporating, in the order of light progression, a 1 m concave collimator mirror, a plane echelle grating and a 1 m concave grating which acts as a camera mirror and cross disperser The system corresponds to an Ebert configuration in the direction of the echelle dispersion, and

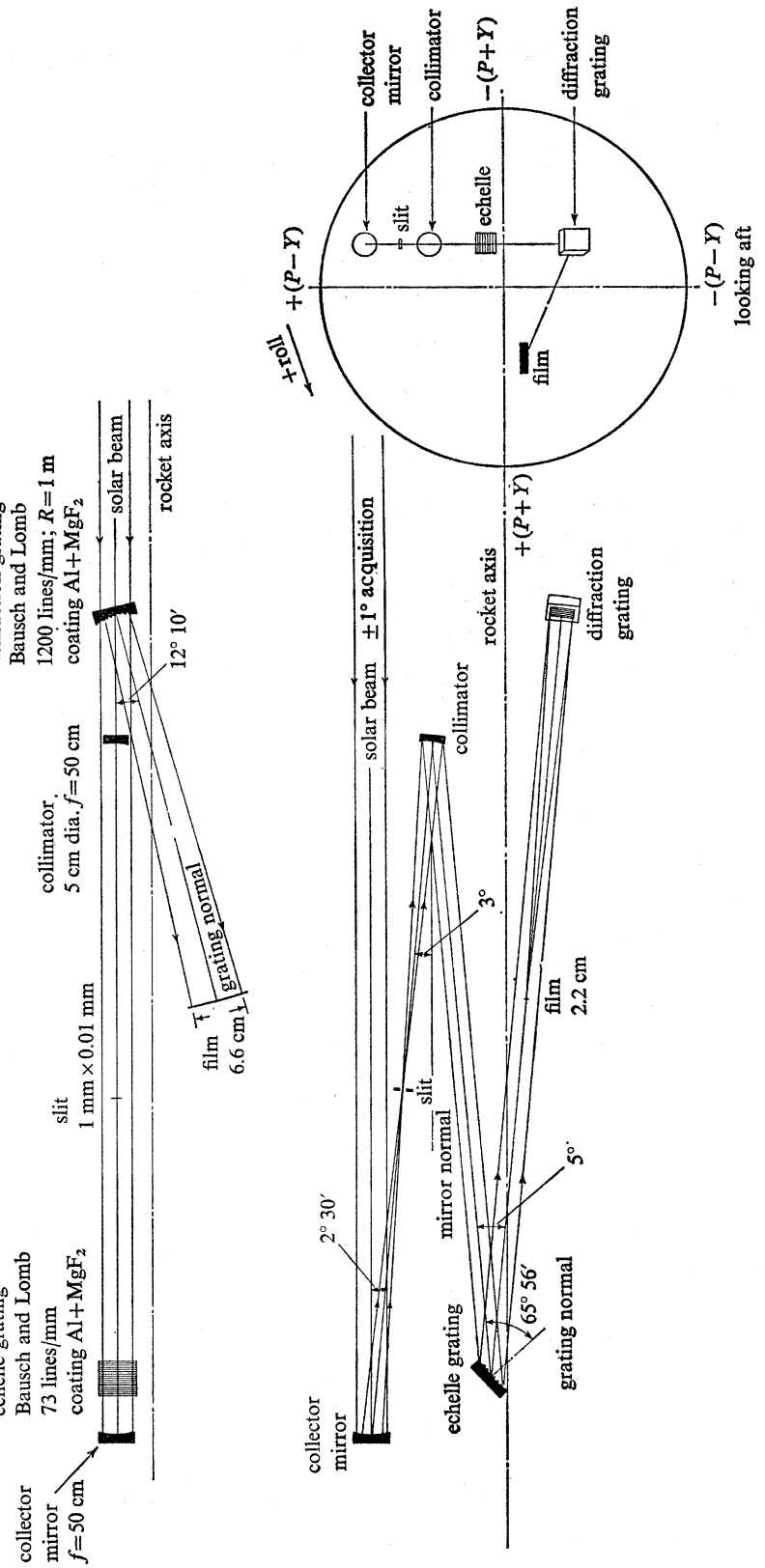

FIGURE 1. Optical layout of rocket-mounted echelle spectrograph.

to a Wadsworth configuration in the direction of the concave grating dispersion. The spectrum is recorded in a two-dimensional format on Kodak 101–01 photographic emulsion.

An optical alinement system (Black & Shenton 1966), incorporating a servo-controlled image forming collector mirror, gave a net stabilization of $\pm 3''$ about the lateral axes in the position of the solar image relative to the spectrograph slit. Roll control of $\pm 2.5°$ was provided by the standard Elliott Automation Ltd. vehicle stabilization unit (Cope 1964). The slit, of length 1.0 mm and width 0.018 mm, was set in the northeast quadrant of the solar image (diameter 4.6 mm), parallel to and 5′ from the north–south axis, with its lower edge 1′ from the equator.

The collector and collimator mirrors were both coated with Ge + Zn S (Hass & Tousey 1959) to discriminate against radiation of longer wavelengths and produce a significant reduction in the scattered light level within the instrument. The echelle and concave grating were coated with $Al + MgF_2$. The linear dispersion of the echelle grating is about 0.1 nm/mm at $\lambda = 200$ nm, and the pre-flight spectral resolution of the instrument was measured as 2 pm in the laboratory.

Results

The spectrum obtained from the 50 s exposure is reproduced in figure 2, plate 1. An examination of the fine detail in this spectrum indicates an in-flight resolution of 3 pm. The discontinuity in the solar intensity around 208.7 nm is evident in the direction of the concave grating dispersion, appearing as a sudden fall from cycle 7 to cycle 8. The analysis will show, however, that the fall is not in the form of a sharp step but that it extends over a range of 1 to 2 nm.

Several broad absorption features with widths up to 0.2 nm are noticeable in most of the echelle cycles. Some of these features coincide with groups of closely spaced iron lines which are strong in laboratory sources. This is illustrated by figure 3, plate 2, which shows the solar spectrum and a laboratory iron spectrum, both taken with the echelle spectrograph, placed in juxtaposition to indicate the coincidences. Most of the other broad features are probably due to similar line clumping. However, this is not true in the case of the broad feature in the lower part of the fifth cycle. This has a measured wavelength at the deepest part of the line of 212.412 nm which coincides with the Si I transition $3p^2\,{}^1D_2$–$3d\,{}^1F^0_3$. The broad profile itself can be seen crossed with a number of sharper absorption lines. Its identification and formation is discussed below.

In general, the average occurrence of an absorption line is every 0.02 nm, and this indicates the maximum interval of what could be considered as the undisturbed continuum level. The number density of lines in each echelle cycle ($\sim$ 1.8 nm spectral range) remains approximately constant up to cycle 7, the number of lines per cycle from cycle 2 through to cycle 7 being 99, 88, 102, 107, 80, 68. On the 100 s exposure the absorption lines can be followed out to cycle 11, with the lines per cycle from cycle 8 through to cycle 11 being 30, 26, 13, 17. The apparent fall in the number of lines per cycle after cycle 7 may, in part, be due to the lower level of photographic density on the film, the weaker lines being difficult to detect above the photographic noise level. However, the intercycle background level is very low in this region and it is unlikely that weak lines have been filled in by background effects. No emission lines can be detected in any part of the observed range.

Photometric reduction

The microphotometry was carried out at Stockholm Observatory using a Krussphotometer which produces the data in digital form for storage on magnetic tape. The photometer scanning

slit corresponded to a width of 30 μm on the film and the output readings were recorded at intervals of 10 μm.

The characteristic curve for the emulsion was measured in the laboratory using separately a continuous radiation source and also a line source. The four exposures recorded on the flight films were also used to construct a characteristic curve. No significant differences were found in comparing the three curves and the in-flight data were adopted. The resulting single characteristic curve was then used to reduce the density measurements to an intensity scale. The assumption of constant energy response for the emulsion over the 20 nm spectral range is well supported by the measurements of Hatter & Ridgeley (1970).

Allowance was made for the effect of background scattered radiation whose level at any wavelength in an echelle cycle was taken as the measured average value of the intercycle background adjacent to the wavelength point. In addition, the instrumental efficiency variation through each echelle cycle over the full wavelength range was accounted for. This was done by using the recovered solar instrument to record a continuous spectrum from a laboratory source having an approximately flat spectral distribution in this region. The reduced solar data were then expressed in terms of the reduced source data at each wavelength to give a ratio independent of instrumental effects but with an intensity unit (the source) which may vary through the wavelength range. To account for this the absolute monochromatic transmission of the instrument was measured over the observed spectral range and together with the constant energy response of the emulsion was used to determine the departure from a flat spectral distribution in the source. This departure amounted to less than 10 % over the whole range, and accordingly, measurements were only made at the maxima of the echelle cycles. The final solar intensity $R(\lambda)$ is then given by

$$R(\lambda) = \frac{I_{\mathrm{s}}(\lambda) - I_{\mathrm{s.b.}}(\lambda)}{f(\lambda)\,[I_{\mathrm{l}}(\lambda) - I_{\mathrm{l.b.}}(\lambda)]}, \tag{1}$$

where $I_{\mathrm{s}}(\lambda)$ and $I_{\mathrm{s.b.}}(\lambda)$ are the reduced intensities derived from the characteristic curve for the solar spectrum and its background, $I_{\mathrm{l}}(\lambda)$ and $I_{\mathrm{l.b.}}(\lambda)$ are the corresponding values for the laboratory source and $f(\lambda)$ is the factor which removes departures from a constant energy distribution in the source. $R(\lambda)$ is then expressed in terms of an arbitrary but constant intensity unit and hence relative intensities throughout the solar spectrum can be derived directly from the final data.

$R(\lambda)$ was computed at intervals of 10 μm through each echelle cycle. A film plotter was then used to reproduce the solar spectrum in an analogue form with relative intensity units along the vertical axis and distance in millimetres through an echelle cycle along the horizontal axis. Figure 4 shows cycles 2 to 8 plotted in this form with a wavelength scale fitted to the horizontal axis. The errors inherent in the method of intensity data reduction have been estimated as a maximum percentage error of $\pm$ 15 % on the intensity plots in each cycle.

From an examination of the spectral data, a number of peak intensities have been selected as being representative of the continuum. These are plotted in figure 5 and reveal the extent in wavelength range and the magnitude of the fall in intensity around 208.7 nm.

Wavelength determination

In the echelle format the relation between wavelength and position on the film is two-dimensional. The echelle and concave grating dispersions vary slowly and independently as the wavelength changes. Harrison has described a method of wavelength determination in echellegrams which operates in $(m\lambda)$ space and uses a fiducial line crossing the entire film in the direction

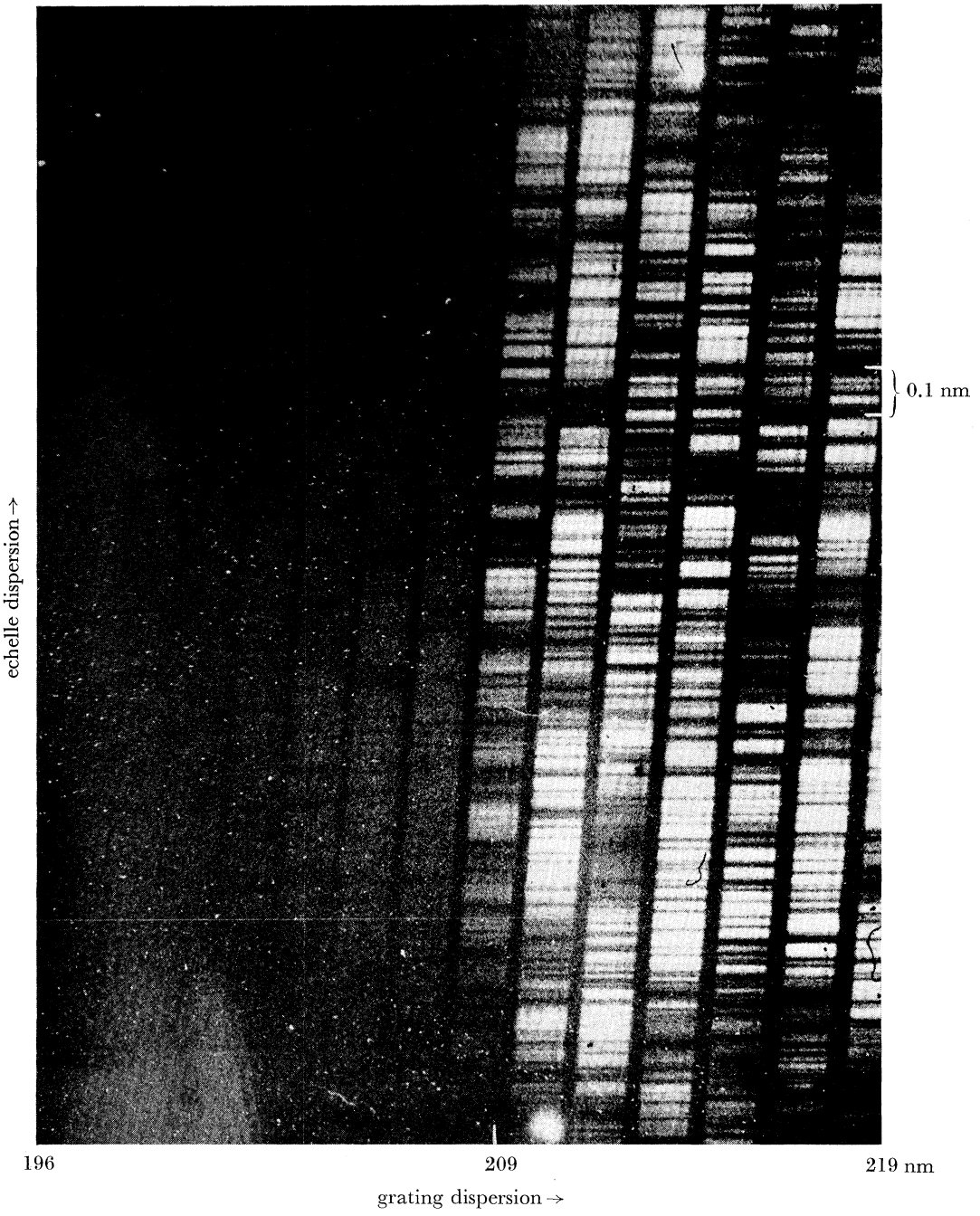

FIGURE 2. High resolution solar spectrum in region 200 to 220 nm in the two-dimensional format of echelle spectrograph.

(*Facing p.* 32)

PHILOSOPHICAL TRANSACTIONS OF THE ROYAL SOCIETY A MATHEMATICAL, PHYSICAL & ENGINEERING SCIENCES

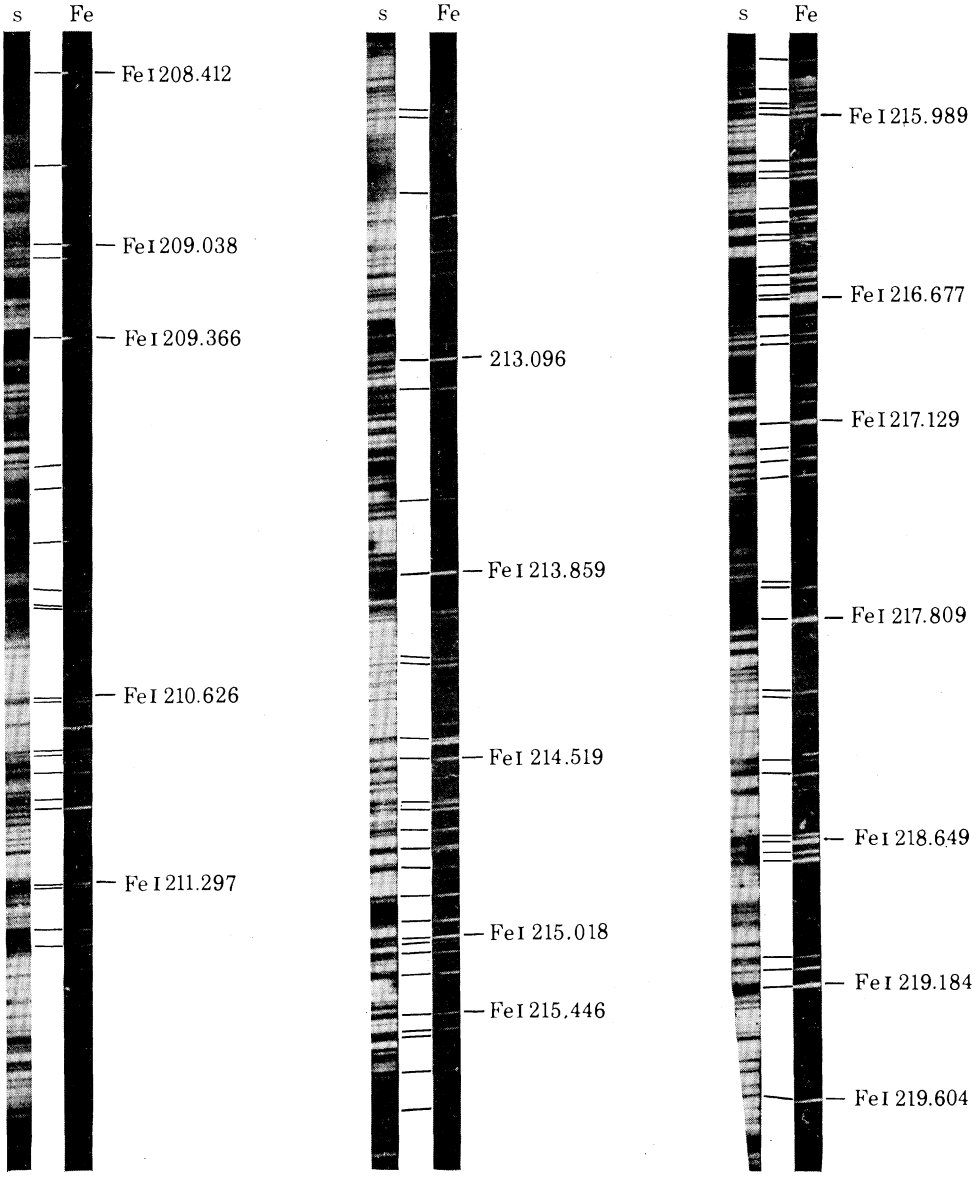

FIGURE 3. Comparison of (s) solar spectrum with (Fe) laboratory Fe source over range 208 to 220 nm using the same instrument. Successive echelle cycles have been joined together.

PHILOSOPHICAL TRANSACTIONS OF THE ROYAL SOCIETY A MATHEMATICAL, PHYSICAL & ENGINEERING SCIENCES

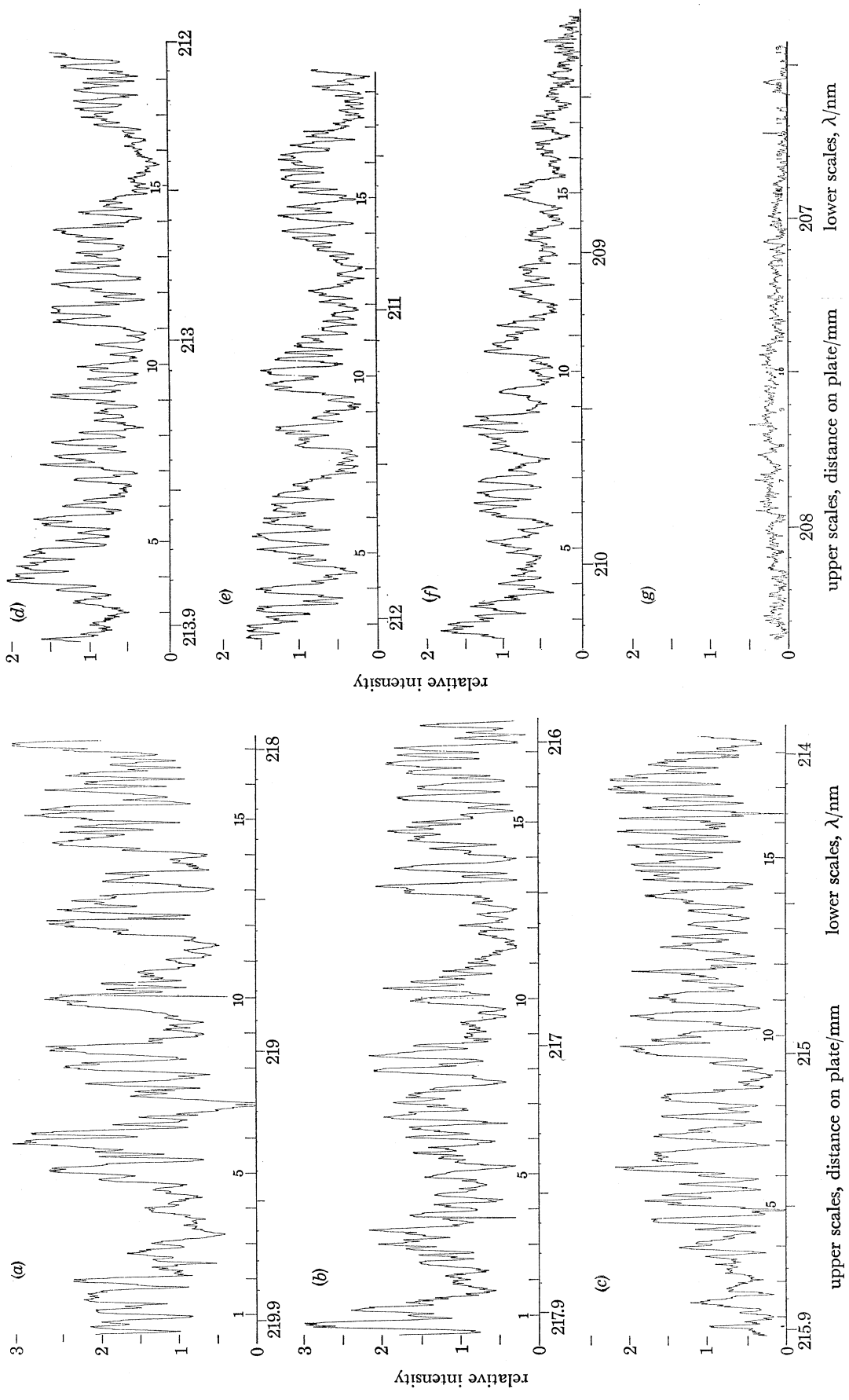

FIGURE 4*a–g*. Intensity plot of solar spectrum in echelle cycles **2** to 8.

of the concave grating dispersion. With this technique high precision wavelength determinations are possible using only two or three well-known standard wavelengths. In the present case, involving a rocket it was not possible to produce a fiducial line across the film. Instead the echelle spectrograph was used to record the spectrum of a laboratory source giving the iron spectrum in

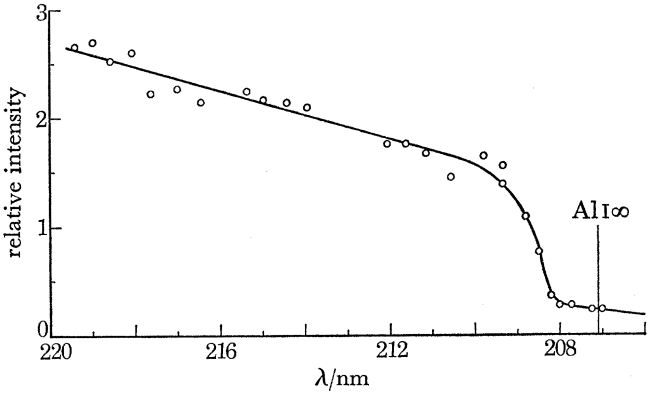

FIGURE 5. Intensity plot of 'continuum' points in solar spectrum over observed wavelength range showing discontinuity near 208.7 nm. This is assigned to the ionization limit of Al I (see text).

the range $\lambda = 200$ to 220 nm. By comparing the solar spectrum with the laboratory iron spectrum it was possible to identify iron lines in each cycle of the solar spectrum and these lines were used as wavelength standards. One identified line in each cycle was chosen to represent a fiducial line for that cycle. A plate factor $m\,\mathrm{d}\lambda/\mathrm{d}l$ was determined by measuring the separation between pairs of close lying standards and this plate factor was then applied to the entire film. If λ_0 is the wavelength of the chosen fiducial line in a particular cycle, then wavelengths of other lines in the cycle are determined from the expression

$$m\lambda = m\lambda_0 \pm ml\,\mathrm{d}\lambda/\mathrm{d}l \pm \epsilon. \tag{2}$$

Here ϵ is an empirically determined correction factor and l is the distance from the fiducial line λ_0, to the line λ. The curve relating ϵ to l and m can be determined using the expression and measuring identified solar iron lines in each cycle.

An alternative method of wavelength determination was also used. Following the previous analysis it was possible to make good identifications for at least six iron wavelengths in each of the cycles 1 to 7. These were then used as standards for a computer-fitted dispersion curve for each cycle, the program making interpolations to yield the wavelengths of the measured lines on the film. The 25, 50 and 100 s solar exposures were measured using the fiducial line method and the 50 s exposure was also measured using the computer fitted dispersion curve. The wavelengths quoted are the mean values of all the measurements.

For well-defined lines on the films the stated wavelength is considered accurate to ± 2 pm in cycles 1 to 7. For the more diffuse lines the accuracy is somewhat less and is mainly dependent on the precision with which the observer can set the cross-wire in the measuring microscope. In these cases the error may amount to as much as 5 pm. For cycles 8 to 11 the available standard wavelengths were more limited in number and the error in these cycles is given as $\pm$ 5 pm.

TABLE 1. OBSERVED WAVELENGTHS AND IDENTIFICATIONS

observed λ/nm	laboratory λ/nm	ion	multiplet number
	cycle 1		
220.6270	220.633	Zr III	40
5943	5886	Co II	10
5716	—	—	—
5469	—	—	—
5216	520	Cr I	43
4929	—	—	—
4467	4482	W II	—
4154	—	—	—
3632	364	Ag II	20
3451	342	Fe II	406
3117	—	—	—
3010	—	—	—
2653	—	—	—
4434	—	—	—
2212	—	—	—
1938	193	Cr III	58
1434	141	Ni II	13
—	146	Cr III	60, 68
1300	—	—	—
1163	1117	Fe I	20
1041	098	Cr III	51
0710	071	Ni I	37
	0728	Fe I	21
0395	0370	Fe I	21
0093	008	Fe I	—
219.9856	—	—	—
9707	9660	V II	201
9358	—	—	—
9181	9183	Al I	8
	917	Zr II	80
8941	891	Cr I	43
8700	875	Co I	23
	8714	Ge I	11
8598	—	—	—
8480	8524	V II	145
8270	8279	CO II	10
8156	815	Mo II	37
	cycle 2		
219.7495	219.748	Mo II	64
7379	7347	Ni I	36
7242	7230	Fe I	20
7001	—	—	—
6813	684	Cr II	151
6743	—	—	—
6283	—	—	—
6630	—	—	—
6436	640	V I	45
6038	6040	Fe I	21
5780	—	—	—
5700	569	V II	201
5590	5532	Fe III	123
5352	—	—	—
5094	5081	Fe III	123
4865	489	Cr I	43
	484	V II	209
4775	—	—	—
4635	—	—	—
4365	—	—	—
4436	—	—	—
4184	—	—	—
3591	3605	Co II	22
	3587	Fe I	—
3374	3411	Fe I	76
3205	—	—	—
2967	—	—	—
2870	—	—	—
2506	—	—	—
2358	—	—	—
2259	2260	Cu II	14
1833	1836	Fe I	21
1591	158	Cr III	51
1357	—	—	—
1311	—	—	—
1202	1215	Fe III	65
	1202	Fe I	22
1070	115	Zr III	40
	110	V I	45
0932	0964	Ni II	29
	092	Cr II	209
0836	083	Cr I	43
0691	—	—	—
0453	048	V II	145
	0444	Mo III	5
0168	—	—	—
218.9879	218.985	W II	—
9773	—	—	—
9657	9621	Cu II	53, 104
9556	—	—	—
9338	933	Co I	119
9130	9183	Fe I	114
8989	—	—	—
8839	—	—	—
8094	809	Cr I	43
	805	Ni II	12
7907	7678	Fe II	135
7608	760	Ni I	16
7493	7444	Fe II	271
7403	739	V I	45
7215	7192	Fe I	21
6896	6890	Fe I	22
6512	6483	Fe I	21
6232	6241	Fe I	20
5986	6030	Co I	81
5909	—	—	—
5699	5654	Fe III	65
5562	551	Ni II	40
5464	539	V II	104, 209
5195	522	Fe I	—
5045	501	Cr III	51, 68
4959	492	Co I	118
4880	489	Mo II	39
4645	4603	Ni II	13
4461	446	Mo II	39

PHILOSOPHICAL TRANSACTIONS OF THE ROYAL SOCIETY A MATHEMATICAL, PHYSICAL & ENGINEERING SCIENCES

TABLE 1 (*cont.*)

observed λ/nm	laboratory λ/nm	ion	multiplet number
	cycle 2 (*cont.*)		
218.4461	218.446	Fe I	—
4279	431	Co I	17
4163	417	V II	145
3976	3979	Fe I	—
3893	391	Ni I	62
3810	3803	Fe II	247
3724	371	Cr III	55, 64
3468	3468	Fe II	119
	3465	Fe I	23
3242	—	—	—
2979	—	—	—
2852	281	Zr II	75
2776	—	—	—
2625	259	Co I	23
2390	238	Ni I	16
2265	—	—	—
2232	222	V I	46
1987	197	V I	46
1731	1729	Co II	11
—	172	Cu I	3
1654	—	—	—
1499	—	—	—
1412	1407	Fe II	370
	141	Cr III	51
1157	1137	F II	370
	1133	Fe I	20
1025	0996	Al I	10
0870	087	Fe II	370
	0866	Fe I	23
0763	074	Cu II	104
0696	—	—	—
0585	0614	Co II	23
0473	0468	Ni II	40
0241	0255	Fe II	370
0060	0060	Co I	20
217.9973	217.999	Ni II	30
9833	—	—	—
	cycle 3		
217.9525	—	—	—
944	217.9454	Ni II	12
9366	9399	Cu II	14
	9348	Ni II	40
8946	8944	Cu I	3
8800	—	—	—
8535	—	—	—
8085	8073	Fe I	21
7677	7690	Fe I	80
7395	743	Si I	91
	7396	Al I	10
	736	Ni II	40
7044	7025	Fe II	106
	700	V I	46
6837	6837	Fe I	23
	6826	Fe II	370
6653	667	Fe I	—
6476	648	Co I	120
6377	6396	Fe I	79
6291	626	As I	19
6201	622	Fe I	—
5972	—	—	—
5472	5445	Fe II	90
5133	5143	Ni II	13
4862	4849	Fe II	135
4660	467	Ni II	14
4487	448	Ni I	36
4295	—	—	—
4089	4113	Al I	9
	4071	Al I	9
3858	3829	Fe III	75
	382	Co I	23
3702	3720	Fe II	79
3536	3535	Ni I	59
3444	345	Fe I	—
3321	3324	Co II	10
3200	3212	Fe I	24
	315	V I	46
2979	2989	Fe II	134
2873	—	—	—
2677	2679	Fe II	372
2587	2581	Fe I	23
2345	2332	Fe I	82
2200	218	Co I	77
2130	2137	Fe I	23
2033	2056	Fe II	372
	2037	Fe I	—
1849	1840	V II	209
	1817	Cu I	26
1556	1550	Fe II	372
	155	Cr II	36
1288	1292	Fe I	24
1071	106	Cr II	36
0768	074	V I	46
	071	Cr II	36
0577	0572	Mo III	5
	055	Co I	23
0167	0193	Fe II	372
216.9962	216.9950	Fe II	370
9853	9843	Al I	—
9580	9562	Cu I	26
9124	9091	Ni II	13
8849	8826	Al I	9
8744	870	Co I	23
8370	8380	Fe I	—
8310	—	—	—
8067	808	V II	29
7882	7880	Fe II	213
7709	770	Si I	92
	768	Cr I	44
7544	—	—	—
7414	7401	Fe II	119
7275	7271	Fe I	78
6765	6769	Fe I	21
6576	6599	Si I	—

TABLE 1 (*cont.*)

observed λ/nm	laboratory λ/nm	ion	multiplet number
	cycle 3 (*cont.*)		
216.6576	216.658	Mo II	39
6192	6198	Fe II	212
	615	Ni I	37
5957	598	Fe I	—
	593	Sr II	3
5870	5860	Fe I	—
5558	555	Ni II	13
	5537	Fe I	80
	552	As I	20
5287	524	Zr II	75
5140	—	—	—
5065	5093	Cu I	4
4876	4915	Al I	—
4569	4577	Al I	—
	4558	Fe II	213
	4547	Fe I	24
4355	4339	Fe II	79
3826	3860	Fe I	24
	3773	Si I	93
3580	356	Co I	23
3370	337	Fe II	372
3037	302	Co I	26
2853	—	—	—
2681	268	Ti II	19
2472	247	Cr I	44
2244	223	Cr I	44
1986	2023	Fe II	90
1643	166	Cr II	133
1573	1582	Fe II	119
	1577	Fe I	27
1259	121	Ni II	14
1176	1161	Fe II	213
1018	104	Ni I	37
0756	—	—	—
0698	—	—	—
0433	0471	Fe II	185
	0383	Al I	—
0222	0236	Fe I	82
	017	Al I	—
	cycle 4		
215.9893	215.992	Fe I	24
9645	9645	Fe I	24
9441	9425	Fe I	27
9153	9152	Fe II	6
8940	8922	Fe I	24
8741	8736	Ni II	13
8520	8518	Fe II	89
8320	831	Ni I	36
	8295	Ti II	19
7950	800	Cr I	44
7806	7792	Fe I	24
7700	774	Cr I	44
7313	—	—	—
705	—	—	—
6964	6955	Co II	11
6826	6804	Ti II	19
6695	6701	Co II	11
6480	6504	Fe I	—
6463	—	—	—
6250	622	Cr II	133
6039	—	—	—
5853	5839	Fe II	213
5638	564	Fe	—
	5598	Ti II	19
5273	5238	Fe I	27, 78
5148	—	—	—
5042	509	Cr I	44
	5012	Fe I	25
4894	—	—	—
4748	470	Ti II	19
4458	4458	Fe I	77
4360	—	—	—
4201	—	—	—
4123	408	Co I	24
3926	3874	Fe II	6
3626	—	—	—
3009	3004	Fe I	27
2842	—	—	—
2573	257	Cr I	44
2378	2373	Fe II	106
2241	228	Cr I	44
	223	Ni I	38
1905	193	Ni I	17
1693	170	Fe	—
1250	—	—	—
1103	1099	Fe I	24, 25
	1095	Fe II	106
0689	0699	Al I	—
0437	043	Si I	95
0182	0182	Fe I	25
214.9624	214.962	Fe I	—
9417	9416	Fe I	81
9148	9170	Fe I	80
	9108	P I	4
8980	8974	Cu II	14
8578	—	—	—
8484	—	—	—
8390	8394	Fe I	29
8230	—	—	—
7907	7911	Si I	94
	7904	Fe III	59
7744	7719	Fe II	213
7539	754	Al I	—
	752	V II	6
7456	—	—	—
7378	—	—	—
7202	719	Cr II	14
7015	704	Fe I	—
6770	681	Fe I	—
6636	—	—	—
6533	—	—	—
6352	6339	Fe III	59
6252	626	Co I	23

TABLE 1 (*cont.*)

observed λ/nm	laboratory λ/nm	ion	multiplet number
	cycle 4 (*cont.*)		
214.6016	214.6058	Fe II	6
	5990	V II	6
5848	—	—	—
5549	5555	Al I	—
5178	5188	Fe I	27
4951	—	—	—
4668	—	—	—
4549	4579	Fe I	81
4407	4408	Cd II	1
4217	—	—	—
4069	408	As I	20
	405	Cr II	14
3893	389	Fe I	—
3696	3706	V II	6
3530	—	—	—
3351	337	Fe I	—
2998	3038	V II	7
2816	282	Fe I	—
2732	274	V II	6
2550	2575	Fe I	—
	252	Ta II	5
2469	244	Mo II	30
2380	240	V II	124
	239	Al I	—
2284	—	—	—
2129	2141	Fe I	30
1985	1973	V II	7
1724	1715	Fe I	25
1463	1471	Fe I	16
1316	—	—	—
1198	—	—	—
1043	1083	Fe I	26
0869	—	—	—
0733	—	—	—
0657	0612	Fe II	212
0477	050	Cr II	14
0269	—	—	—
0178	—	—	—
0098	0064	V II	7
213.9876	213.9929	Fe I	29
9750	9798	V II	7
	cycle 5		
213.9630	213.9676	Fe II	6
9310	933	Cr II	17
	929	Mo II	43
9179	—	—	—
9048	898	Co I	28
8534	8589	Fe I	24
	856	Zn I	1
8145	817	V II	7
	8103	Fe II	135
8024	—	—	—
7737	7735	Fe II	6
7479	—	—	—
7267	731	V II	7
7030	—	—	—
6909	—	—	—
6699	—	—	—
6435	—	—	—
6165	6199	P I	4
5948	5976	Cu II	14
5700	—	—	—
5430	5466	P I	4
	542	Cr II	23
5299	534	Cr II	23
5081	509	Cr II	23
4875	488	Cr II	23
4747	4733	Al I	—
4602	462	Cr II	23
	4592	Fe II	212
4500	452	Cr II	23
4474	—	—	—
4263	428	Ni II	31
4128	412	V II	7
3971	3990	Fe II	213
3803	381	Cr II	23
	380	As I	20
3707	—	—	—
3463	349	Cr II	23
3313	3311	Fe I	81
2995	303	Cr II	24
2914	293	Cr II	24
2719	276	Co I	23
	271	Cr II	27
2683	—	—	—
2351	238	Cr II	27
	2304	Ca II	3
2184	—	—	—
2015	2015	Fe I	25
1844	1898	Ru II	85
1523	1505	Ca II	3
1371	—	—	—
1277	127	Ni II	14
1067	106	Co I	29
0983	102	Ni II	31
0756	0762	Cu I	21
0528	0548	Fe II	249
0421	042	V II	180
	0417	Fe I	83
0209	0259	Fe II	80
	022	Cr II	14, 24
212.9932	212.996	Ni I	37
	989	Cr II	24
9708	9663	Al I	—
9537	—	—	—
9175	914	Ni II	31
8877	—	—	—
8821	8836	Ru II	79
8727	—	—	—
8559	857	Ni II	15
8382	841	Ni I	19
8145	—	—	—
7915	7967	Fe II	290

PHILOSOPHICAL TRANSACTIONS OF THE ROYAL SOCIETY A MATHEMATICAL, PHYSICAL & ENGINEERING SCIENCES

TABLE 1 (*cont.*)

observed λ/nm	laboratory λ/nm	ion	multiplet number
	cycle 5 (*cont.*)		
212.7761	212.777	Ni II	41
7624	—	—	—
7481	7467	Fe I	28
7295	730	Al I	—
	727	Mo II	43
7148	714	Co I	80
6999	—	—	—
6812	—	—	—
6513	646	Mo II	15
6237	6212	Fe I	27
6098	—	—	—
5859	589	Ni II	13
5646	562	Ni I	16
5433	—	—	—
5324	532	Co I	28
5219	—	—	—
5134	512	Ni II	14
4959	4948	Fe I	—
4809	480	Ni I	63
4529	—	—	—
4117	4122	Si I	48
3343	3362	Al I	—
3133	3118	Fe I	—
2991	2994	Si I	49
2791	—	—	—
2655	267	Co I	77
2566	—	—	—
2449	241	Zr II	75
2242	225	Ni I	41
2173	2188	Fe I	26
1958	—	—	—
1864	—	—	—
1640	160	W I	4
1569	159	Al I	—
	154	V II	172
1385	140	Ni I	38
1233	—	—	—
1177	1195	Si I	4
1064	—	—	—
0747	070	Co I	28
0509	053	Mo II	15
0382	—	—	—
0238	—	—	—
0057	—	—	—
211.9887	211.991	Co I	80
9767	971	Mo II	15
9637	—	—	—
9217	9192	Co I	—
9150	9125	Fe I	28
	cycle 6		
211.9050	211.9050	Fe II	120
8946	—	—	—
8659	865	Cr III	70
8521	851	Co I	80
8285	831	Al I	—
8121	—	—	—

observed λ/nm	laboratory λ/nm	ion	multiplet number
	cycle 6 (*cont.*)		
7759	768	Co I	86
7039	—	—	—
6825	683	Co I	24
6786	677	Mo II	31
6678	—	—	—
6527	656	Al I	—
6255	—	—	—
5741	—	—	—
5553	—	—	—
5342	535	Co I	80
5168	5168	Fe I	33
4947	495	Al I	—
4764	—	—	—
4588	4588	Fe I	33
4353	—	—	—
4135	—	—	—
3967	—	—	—
3598	—	—	—
3341	—	—	—
3153	319	Ca II	9
	308	Fe I	81
2996	2966	Fe I	33
2792	2763	Ca II	9
2638	—	—	—
2459	242	Al	—
2172	216	Cr II	15
1736	173	Ni I	17
1450	1470	Co II	2
1256	126	Cr II	26
	122	Fe I	31
1118	—	—	—
0993	098	Cr II	26
0919	092	Cr II	26
0731	0727	Fe II	108
0463	—	—	—
0233	0240	Fe II	290
	0233	Fe I	83, 31
210.9939	210.994	Mo II	43
	995	Al	—
9768	979	Ni I	17
9605	966	Zr II	60
	958	Si I	—
9276	927	V II	156
9084	9097	Fe II	227, 250
8954	8955	Fe I	33
	8942	Fe II	227
8676	8676	Fe III	105
8590	858	Al	—
8303	8302	Fe I	34
8139	8139	Fe I	81
7944	794	Ni II	60
	792	Cr II	16
	787	Al	—
7795	—	—	—
7527	755	Al I	—
7267	721	Ni I	62
7164	—	—	—

PHILOSOPHICAL TRANSACTIONS OF THE ROYAL SOCIETY A MATHEMATICAL, PHYSICAL & ENGINEERING SCIENCES

TABLE 1 (*cont.*)

observed λ/nm	laboratory λ/nm	ion	multiplet number
	cycle 6 (*cont.*)		
210.6825	210.682	Co I	90
6688	—	—	—
6380	638	Fe I	33
6264	626	Fe I	31
6063	—	—	—
5833	5824	Ge I	3
	583	Zr I	19
5503	—	—	—
5347	5394	W I	4
5134	5112	Cu I	23
4850	484	V I	49
4763	478	Cu II	15
4426	—	—	—
4144	—	—	—
3992	3967	Fe I	31
3753	3799	Fe III	66
3644	363	Al	—
3444	343	Mo II	19
	339	Ni II	31
3269	3239	Ca II	9
	321	Si I	—
3048	3048	Fe I	31
2938	2910	Fe I	34
2707	—	—	—
2352	2349	Fe I	33
2200	223	V I	47
1863	186	V II	156
1667	—	—	—
	cycle 7		
210.1550	210.1538	W I	—
1348	—	—	—
1166	117	V II	94
0925	0963	Fe II	250
	096	Cr II	16
0681	070	Mo II	19
0490	051	V I	48
0444	—	—	—
0300	034	Cr II	16
0256	—	—	—
0240	—	—	—
0108	0144	Fe I	34
209.9970	—	—	—
9735	—	—	—
9221	209.9231	Fe III	66
8953	8953	Fe I	34
8926	893	Co I	28
8526	850	V I	47
8288	—	—	—
8084	8081	Fe I	31
7906	—	—	—
7451	7512	Fe II	80
	7480	Fe III	67
7335	734	V I	48
7031	708	Ni II	31
	699	Fe II	91
6678	672	V I	49
	663	Al I	—
6177	619	V I	47
5752	577	V I	49
	575	Ni I	18
5611	—	—	—
5452	5451	Fe I	31
5274	529	Mo II	19
4939	493	Cr I	2
4837	486	Co I	86
	479	Al II	—
4637	—	—	—
4278	426	Al II	—
4062	—	—	—
3699	3683	Fe II	290
	3660	Fe I	33
3529	355	Ni II	15
	3504	Fe III	77
3395	340	Co I	86
3146	311	Mo II	19
2838	288	Zr I	19
2666	264	Mg III	6
2515	—	—	—
2201	—	—	—
1942	198	Co I	88
1718	169	Ni I	39
1110	—	—	—
0877	0862	Fe I	34
0641	064	V I	48
0383	0380	Fe I	31
0112	0140	Ni II	15
	0139	Fe III	67
208.9903	208.994	V I	—
9747	974	As I	90
9578	957	B I	2
	953	Mo II	19
9105	912	Cr II	16
	909	Ni I	19
	9089	Fe III	77
8910	884	B I	2
8590	856	V I	49
8110	—	—	—
7911	793	Cu II	94
7547	7527	Fe II	108
	7525	Fe I	34
7281	—	—	—
6992	70	Al II	3
6741	678	Zr III	8
6204	—	—	—
5822	—	—	—
5665	—	—	—
5370	537	Ni I	41
4483	4467	Si I	50
4114	412	V I	49
	4117	Fe I	33
3686	365	Ni II	14

PHILOSOPHICAL TRANSACTIONS OF THE ROYAL SOCIETY A MATHEMATICAL, PHYSICAL & ENGINEERING SCIENCES

TABLE 1 (*cont.*)

observed λ/nm	laboratory λ/nm	ion	multiplet number
	cycle 8		
208.332	—	—	—
274	208.2692	Co II	18
238	—	—	—
200	201	Si I	51
154	15	Al II	3
115	—	—	—
090	—	—	—
032	0276	Fe II	92
207.970	—	—	—
893	207.8989	Fe III	48
811	8167	Fe II	91
755	7507	Fe II	136
688	687	V II	—
617	—	—	—
540	—	—	—
498	—	—	—
418	4195	Fe II	91
	413	Ni II	42
345	—	—	—
298	—	—	—
249	243	V II	173
218	226	Ni I	21
150	—	—	—
102	—	—	—
050	0539	Fe III	99
206.997	—	—	—
876	206.880	V II	173
788	7917	Fe II	137
731	7302	Fe III	124
662	666	Cr II	52
640	641	Ni II	15
	cycle 9		
206.602	206.6005	Fe II	109
540	535	Zr II	76
487	486	Co I	86
436	439	Ni I	40
365	3672	Fe II	92
324	321	Cr II	52
297	—	—	—
249	—	—	—
208	—	—	—
106	103	Cr II	248
078	076	Ni I	39
039	—	—	—
205.970	205.9677	Fe III	78
901	9014	Si II	—
871	8646	Si II	—
817	8136	Si I	52
669	—	—	—
645	—	—	—
616	6148	Co III	65
	6145	Fe III	71
572	—	—	—
543	550	Ni I	19
483	481	Si I	5
	485	V II	—
461	—	—	—
424	—	—	—
333	330	Ni II	15
305	3108	Co III	65
	cycle 10		
204.285	204.278	Cr II	135
191	—	—	—
000	203.993	Al	—
	995	Co I	92
203.979	984	Zr II	76
957	—	—	—
877	885	V I	50
831	—	—	—
800	—	—	—
673	—	—	—
628	—	—	—
587	5845	Cu II	15
399	406	V I	50
315	—	—	—
	cycle 11		
202.646	202.651	Co I	37
467	—	—	—
405	—	—	—
373	3715	Fe II	187
167	—	—	—
092	098	Ni II	43
201.955	—	—	—
923	—	—	—
883	201.8772	Fe II	94
843	—	—	—
755	748	Cr II	17
698	691	Al	—
666	—	—	—
586	587	Al	—
	587	Cr II	30
	586	Zr II	54
554	5500	Fe II	83
530	—	—	—
273	274	Cr II	249

Line identifications

The measured observed wavelengths are tabulated under their cycle number in table 1 with proposed identifications based on listed laboratory spectra (Moore, 1952; Harrison 1956; Junkes, Salpeter & Milazzo 1965) or on near coincidences with calculated wavelengths. Where the identification is based on the ultraviolet multiplet tables the multiplet number is indicated and

these same tables provided the wavelength source for the lines used as standards. Of the 663 lines listed, nearly 90 % have proposed identifications.

Two striking features in the observed spectrum are the strong discontinuity in the continuous spectrum near 208.7 nm and the broad absorption feature at 212.4 nm. The former is classified as the photoionization edge of Al I and the latter as a Si I line. An analysis of the formation of these features has been carried out, mainly with the view of confirming their identification.

Absorption edge at $\lambda \approx 208.7$ nm

The general level of the observed spectrum shows a rapid decrease in intensity from $\lambda \approx 210$ nm down to $\lambda \approx 208$ nm (figure 5). The intensity is estimated to drop by a factor five.

The discontinuity was first discovered by Johnson, Malitson, Purcell & Tousey (1958). Kodaira (1965), using old observational data which gave an intensity drop of a factor of two, concluded that the photoionization from the ground state ($3p\,^2P$) of neutral aluminium was responsible. Bonnet, Blamont & Gildwarg (1967) observed an intensity drop of a factor 5–6 at the disk centre which fell to an undetectable level at the limb. They deduced an opacity which was a factor 3–5 higher than they computed for Al I using the abundances of Goldberg, Muller & Aller (1960) and a photoionization cross-section of 12×10^{-18} cm^2. They drew no specific conclusions because of the uncertainty level of a factor of two in the value of the cross-section.

In the present analysis the Bilderberg model of the photosphere and low chromosphere (Gingerich & de Jager 1968) and the abundance of Goldberg *et al.* (1960) were used together with the opacities of Travis & Matsushima (1968) who used the quantum defect method to calculate the photoionization cross-sections of various elements. Their value for the photoionization cross-section of Al I is 22×10^{-18} cm^2 in good agreement with the experimental determinations of Kelm and of Parkinson & Reeves (see Gingerich & Rich 1968). Travis & Matsushima's calculations show that near $\lambda = 210$ nm the important opacity sources in the Sun are due to H, H^-, Mg I and Al I (see also Matsushima 1968).

On the above basis, calculations were made of the emergent solar flux above and below the discontinuity which gave values in good agreement with those of Gingerich & de Jager (1968) using the Bilderberg model and the opacities of Gingerich & Rich (1966, 1968). By matching these calculations with the observations for wavelengths above the discontinuity a theoretical 'calibration' of the observed spectrum was possible which gives 0.95 J cm^{-2} s^{-1} sr^{-1} nm^{-1} for the intensity unit in figures 4 to 6. Using this value for the intensity unit and extrapolating the observed spectrum (figure 5) above the discontinuity down to the Al I $3p\,^2P_{\frac{1}{2}}$ edge at $\lambda = 207.1$ nm gives an intensity of 1.2 J cm^{-2} s^{-1} sr^{-1} nm^{-1}. Similarly, the value at the edge but below the discontinuity is 0.23 J cm^{-2} s^{-1} sr^{-1} nm^{-1}. This latter value is a factor of 2.5 smaller than obtained theoretically. Hence, the observed intensity ratio across the edge of 5.0 compares with the theoretical prediction of 2.0.

Before discussing this disagreement, the observed wavelength position of the edge will be considered. A precise theory of the absorption coefficient does not exist in the domain where the perturbed high levels partially overlap. Hence, approximate calculations have been made with the restricted aim of determining the position of the edge. This is best defined by the wavelength at which absorption is effectively complete (observed at 208 nm—see figure 5) for which the generally adopted criterion is

$$E_{n+1} - E_n = \Delta E_n, \tag{3}$$

where E_{n+1} and E_n are the energies of successive levels in the system and ΔE_n is the half width of

level n due to Stark broadening. Since we are dealing with high lying levels in a neutral atom hydrogenic expressions can be used for E_n and linear Stark theory for ΔE_n.

There are some divergences in the literature for the expression for ΔE_n. Whereas Griem (1964) gives a value which is twice the original one derived by Inglis & Teller (1939), laboratory measurements (Vidal 1966) give results in good agreement with it. The Inglis–Teller formula was therefore adopted to give

$$\Delta E_n = 11.1 n^2 a_0 e^2 N^{\frac{2}{3}}, \tag{4}$$

where a_0 is the first Bohr radius, e the electron charge and N the number density of electrons and ions ($N = 2N_e$).

Equations (3) and (4) can be combined to give

$$(\lambda' - \lambda_\infty)/\lambda' = 2.62 R a_0^{\frac{4}{3}} \lambda_\infty N^{\frac{4}{15}}, \tag{5}$$

where λ' is the wavelength at which level merging should be complete, λ_∞ is the unperturbed photoionization wavelength and R is the Rydberg constant.

Similarly, one can approximately determine the wavelength λ'' of onset of the absorption where merging of levels begins by adopting the criterion

$$E_{n+1} - E_n = 3\Delta E_n \tag{6}$$

to give

$$(\lambda'' - \lambda_\infty)/\lambda'' = 4.06 R a_0^{\frac{4}{3}} \lambda_\infty N^{\frac{4}{15}}. \tag{7}$$

The application of equations (5) and (7) to the solar atmosphere can only be made via the model. This shows that $\lambda'(\text{Sun}) = 208.9$ nm at which wavelength level merging starts at $\tau^- = 0.15$ and is complete by $\tau^- = 0.8$, τ^- being the optical depth for wavelengths longer than the discontinuity. The observed wavelength for completion of the absorption is 208 nm and hence the predicted shift (1.8 nm) is twice that observed (0.9 nm). Even accounting for the approximate nature of this calculation, such a discrepancy is large enough to be considered real.

In principle, it is possible to apply the same analysis as above to determine the wavelength of onset of the edge absorption. In actual fact this takes the calculations beyond the limit of validity of linear Stark theory due to the increased fine structure separation in the levels.

The discrepancy between theory and observation for the intensity drop and wavelength position of the Al I discontinuity will now be examined, starting with the former. The calculations of emergent flux described above show that the important regions for production of the radiation at wavelengths above and below the discontinuity overlap to a large extent. Hence, the discrepancy of a factor of 2.5 in the intensity drop cannot be explained by increasing the temperature gradient, either in the model itself or by postulating an additional overall source of opacity which would raise the formative zones to a region with steeper temperature gradient. The explanation must therefore lie in an increased optical depth beyond the discontinuity. The possibility of an error in the Al I photoionization cross-section derived by Travis & Matsushima (1968) is discarded because of experimental confirmation (see above) leaving only the possibility of a higher population in the ground level population of Al I. This can only be achieved by changes in either the Al abundance or the ionization level.

If the full discrepancy is assigned to the Al abundance then a value of $\lg N(\text{Al}) = 6.60$ on a scale $\lg N(\text{H}) = 12.0$ is derived. This compares with the adopted value of 6.20 derived by Goldberg *et al.* (1960) and the later value of 6.40 obtained by Lambert & Warner (1968*a*) from the analysis of the equivalent widths of 19 lines in the visible and infrared regions of the solar spectrum.

If we now assign the full discrepancy to a change in the Al ionization level it is necessary to consider the effect of temperature changes in the Bilderberg model. For a mass element of dm within the atmosphere, the ionization balance of Al is given by the Saha equation.

$$\frac{\mathrm{d}N(\mathrm{Al\,II})\,\mathrm{d}N_e}{\mathrm{d}N(\mathrm{Al\,I})} = \text{const.}\ T^{\frac{3}{2}}10^{-\chi(\mathrm{Al})\theta}\,\mathrm{d}V \tag{8}$$

where the values dN refer to the total population of the indicated species within the mass element dm whose volume is dV at temperature T K; χ(Al) is the ionization potential of Al in eV and $\theta = 5040/T$. The second stage of ionization is negligible, i.e. $\mathrm{d}N(\mathrm{Al\,III}) \approx 0$.

We now consider a small change in temperature from θ to $(1+q)\,\theta$ and neglect changes of the same order as q. In the region of importance ($\tau_{5000} < 0.2$) the main sources of free electrons are Mg and Si, i.e. $\mathrm{d}N(\mathrm{Mg\,II}) + \mathrm{d}N(\mathrm{Si\,II}) \approx \mathrm{d}N_e$. Further, since $\mathrm{d}N(\mathrm{Mg\,II}) \gg \mathrm{d}N(\mathrm{Mg\,I})$ and $\mathrm{d}N(\mathrm{Si\,II}) \gg \mathrm{d}N(\mathrm{Si\,I})$, then $\mathrm{d}N_e \approx$ constant. Similarly, since $\mathrm{d}N(\mathrm{Al\,II}) \gg \mathrm{d}N(\mathrm{Al\,I})$, then

$$\mathrm{d}N(\mathrm{Al\,II}) \approx \text{constant}.$$

Finally, from the requirement of constant pressure, the constancy of dN_e implies the constancy of dV. In other words, within the particular domain, only dN(Al I) is a sensitive function of temperature and the other variables in equation (8) can be regarded as constant. Hence, for a small temperature change $\theta \to (1+q)\,\theta$, the change in the Al I population is given by:

$$\frac{\mathrm{d}N(\mathrm{Al\,I};\,(1+q)\,T)}{\mathrm{d}N(\mathrm{Al\,I};\,T)} = 10^{-\chi(\mathrm{Al})q\theta}. \tag{9}$$

Since θ is near unity, this expression shows that the intensity drop at the Al I edge is a very sensitive function of the temperature of the layers forming it. Its study is therefore important as a means of checking or modifying solar models in the particular region ($\tau_{5000} < 0.2$). For the same reason, the intensity drop presents an inaccurate means of deriving an Al abundance and we conclude that the discrepancy in the predicted intensity drop can be explained by a slightly lower temperature in the relevant regions of the Bilderberg model.

A proper theoretical fit now requires a reconstruction of the solar model. This has not been carried out to date, but rough calculations indicate that a fit should be possible on the basis of the Lambert & Warner abundance (6.40) and a temperature decrease of 5 % in the Bilderberg model in the region $0.001 < \tau_{5000} < 0.2$.

If we now consider the discrepancy in the wavelength position of the edge, this can only be explained by a decrease of about an order of magnitude in the electron density of the layers responsible for its production. The decrease in temperature in the upper layers of the Bilderberg model, proposed above to explain the intensity drop, has the effect of raising the level at which the edge is produced and, consequently, of reducing the electron density. Again, a proper fit requires a reconstructed model but once more a rough calculation has been carried to test the validity of the proposal. Since the drop in the temperature of the Bilderberg model in the particular region ($0.001 < \tau_{5000} < 0.2$) does not significantly change the electron density, the calculations have been made using Bilderberg densities but with the additional Al opacity resulting from the decrease in temperature. In the first calculations (Bilderberg model, Goldberg *et al.* abundances) complete merging of the Al I levels occurred at 208.9 nm for $\tau^- = 0.8 (\tau_{5000} = 1.2)$. The corresponding electron density is $N_e = 10^{14}\,\mathrm{cm}^{-3}$. For the additional opacity in the modified model, the same situation occurs at $\tau_{5000} = 0.5$ with a corresponding value of $N_e = 2.5 \times 10^{13}\,\mathrm{cm}^{-3}$. In terms of the wavelength position of the edge this now becomes 208.4 nm compared to the

observed value of 208 nm. In view of the approximate nature of the calculations, this discrepancy is considered to be within the errors of estimation.

It is concluded that a decrease in temperature in the region $0.001 < \tau_{5000} < 0.2$ of the Bilderberg model is sufficient to explain the intensity drop and shift of the Al I absorption edge. A more rigorous fit should lead to an improvement of the model in this region.

Absorption feature at $\lambda = 212.4$ nm

The intensity plot covering the broad absorption feature at $\lambda = 212.4$ nm is reproduced in figure 6. An examination of the line identifications in this region (see table 1) seems to rule out line 'clumping' as a possible explanation. Although crossed by several sharper lines, these are sufficiently separated to reveal the background profile of the feature, the symmetry and shape of which suggests a single origin for the feature. A construction of its profile and neighbouring continuum gave an equivalent width and estimated error of 0.16 ± 0.025 nm.

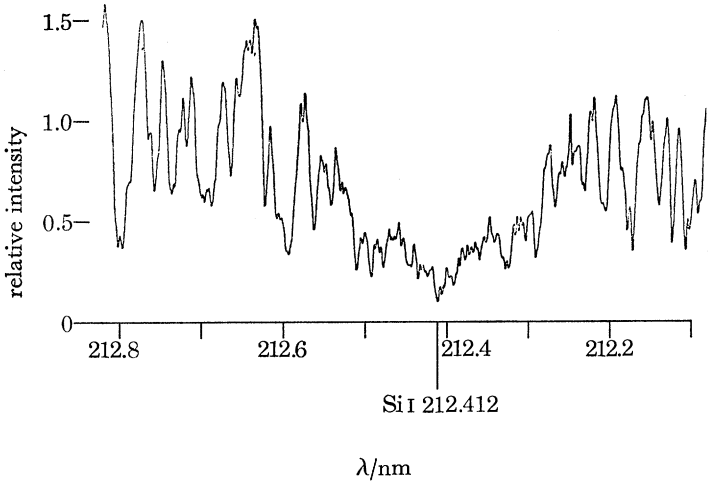

FIGURE 6. Intensity plot of solar spectrum in the neighbourhood of the broad feature at 212.4 nm. This is assigned to Si I (see text).

Since the centre of the feature is coincident with the line of Si I($3p^2\,{}^1D_2$–$3d\,{}^1F^0_3$) at 212.412 nm, an estimate of its expected strength in the solar atmosphere has been carried out to test this identification. A curve of growth method was employed using the data of Wrubel (1950) which are based on Chandrasekhar's exact solution of the transfer equation for the Milne–Eddington model in the case of scattering. For the mean parameters of the layers effective in producing the line, the values corresponding to $\tau_{5000} = 0.3$ in the Bilderberg model were adopted, i.e.

$$T = 5600\,\mathrm{K}, \quad P_e = 1\,\mathrm{N\,m^{-2}}, \quad N_H = 4.25 \times 10^{23}\,\mathrm{g^{-1}}.$$

Using the oscillator strength given by Corliss & Bozman (1962) and the absorption coefficient of Travis & Matsushima (1968), the observed equivalent width can be explained with a Si abundance of $\lg N(\mathrm{Si}) = 7.85 \pm 0.31$. This error should be written up to 0.4 to account for errors in the adopted parameters. The corresponding value derived for the photosphere by Goldberg *et al.* (1960) is 7.50 and by Lambert & Warner (1968*b*) is 7.55, whereas Jordan (1966) derived 7.70 from an analysis of the extreme u.v. emission spectrum. The value derived here agrees with these values within the errors of estimation and it is concluded that the feature is produced by the particular line of Si I.

We are grateful to Mr D. B. Shenton and the Projects Group at Culham who engineered the payload to their usual high standard; and to the Groups at Elliott Bros, Frimley, and British Aircraft Corporation at Filton and Salisbury, South Australia, who were responsible for the technology of the rocket and its operation. On the scientific side, we express our gratitude to Mr N. Carlborg and Mr P. Brattlund (Stockholm Observatory), operating under a contract from the Swedish Space Committee, for their patient work on the data reduction; to Mr C Miccinesi (Arcetri, Florence) for valuable assistance with the analytical calculations; and to Mr P. Monk (Culham) for experimental support throughout.

References (Boland *et al.*)

Black, W. S. & Shenton, D. B. 1966 *Peaceful uses of automation in outer space*, p. 152. New York: Plenum Press.
Bonnet, R. W., Blamont, J. E. & Gildwarg, P. 1967 *Astrophys. J. Lett.* **148**, L115.
Cope, P. E. G. 1964 *J. Br. Interplanetary Soc.* **19**, 285.
Corliss, C. H. & Bozman, W. R. 1962 *Experimental transition probabilities*, N.B.S. Monograph no. 53.
Detwiler, C. R., Garrett, D. L., Purcell, J. D. & Tousey, R. 1961 *Ann. Geophys.* **17**, 263.
Gingerich, O. & de Jager, C. 1968 *Solar Phys.* **3**, 5.
Gingerich, O. & Rich, J. 1966 *Astr. J.* **71**, 161.
Gingerich, O. & Rich, J. 1968 *Solar Phys.* **3**, 82.
Griem, M. R. 1964 *Plasma spectroscopy*, p. 125. McGraw-Hill.
Goldberg, L., Muller, E. A. & Aller, L. H. 1960 *Astrophys. J.* (Suppl.) **5**, 1.
Harrison, G. R. 1956 *M.I.T. wavelength tables*. New York: Wiley.
Harrison, G. R., Davies, S. P. & Robertson, H. J. 1953 *J. opt. Soc. Am.* **43**, 853.
Hass, G. & Tousey, R. 1959 *J. opt. Soc. Am.* **49**, 593.
Hatter, A. T. & Ridgeley, A. 1970 Internal A.R.U. (Culham) Memorandum.
Inglis, D. R. & Teller, E. 1939 *Astrophys. J.* **90**, 439.
Johnson, F. S., Malitson, H. H., Purcell, J. D. & Tousey, R. 1958 *Astrophys. J.* **127**, 80.
Jordan, C. 1966 *Mon. Not. R. astr. Soc.* **132**, 463.
Junkes, J., Salpeter, E. W. & Milazzo, G. 1965 *Atomic spectra in the vacuum ultraviolet*. Specola Vaticana.
Kodaira, K. 1965 *Z. Astrophys.* **60**, 240.
Lambert, D. L. & Warner, B. 1968*a* *Mon. Not. R. astr. Soc.* **138**, 181.
Lambert, D. L. & Warner, B. 1968*b* *Mon. Not. R. astr. Soc.* **138**, 213.
Matsushima, S. 1969 *Astrophys. J.* **154**, 715.
Moore, C. E. 1952 N.B.S. Circular 488, §2.
Travis, L. D. & Matsushima, S. 1968 *Astrophys. J.* **154**, 689.
Vidal, C. R. 1966 *J. Quant. Spectrosc. Radiat. Transfer* **6**, 461.
Wrubel, M. H. 1950 *Astrophys. J.* **111**, 157.

PHILOSOPHICAL TRANSACTIONS OF THE ROYAL SOCIETY A MATHEMATICAL, PHYSICAL & ENGINEERING SCIENCES

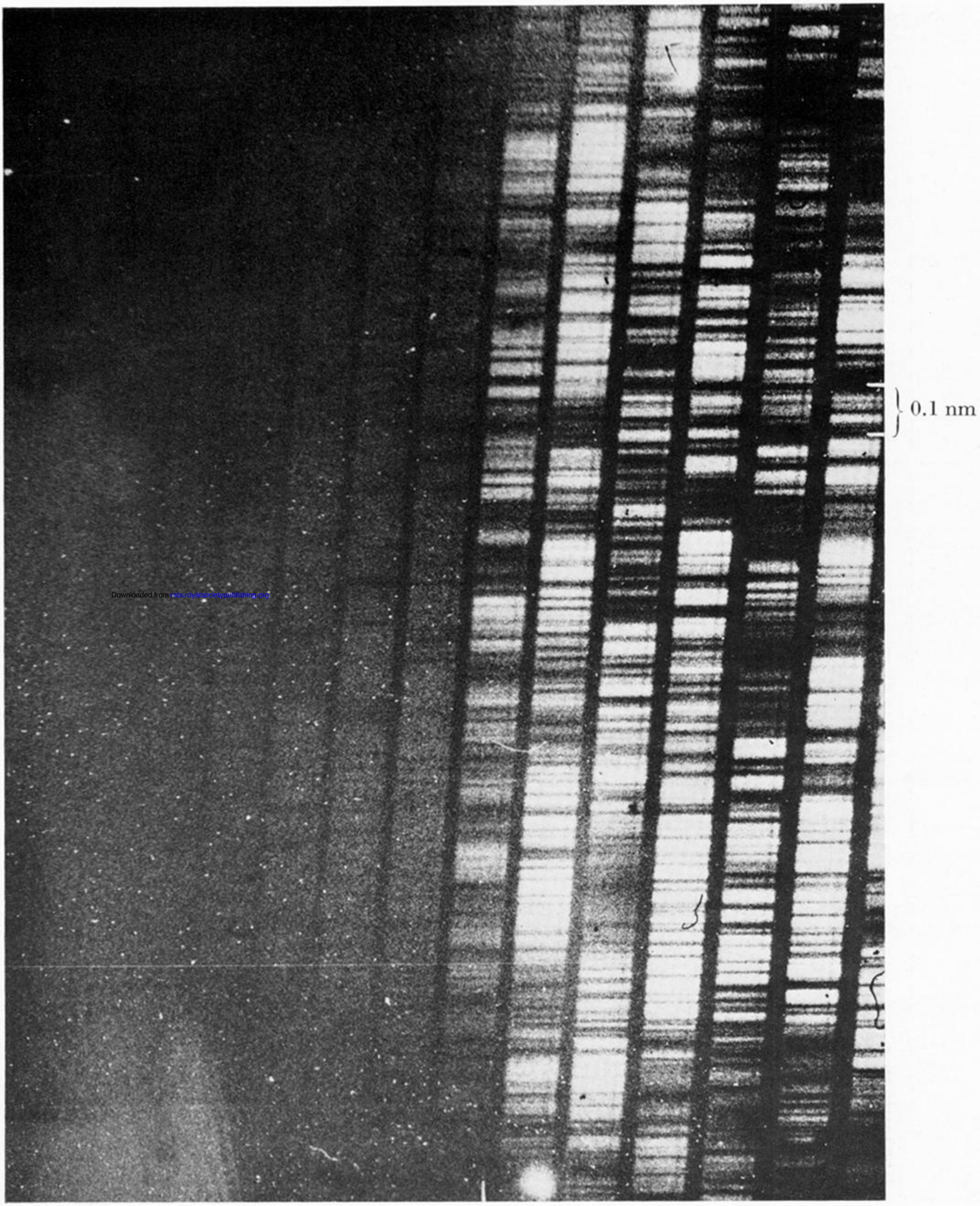

FIGURE 2. High resolution solar spectrum in region 200 to 220 nm in the two-dimensional format of echelle spectrograph.

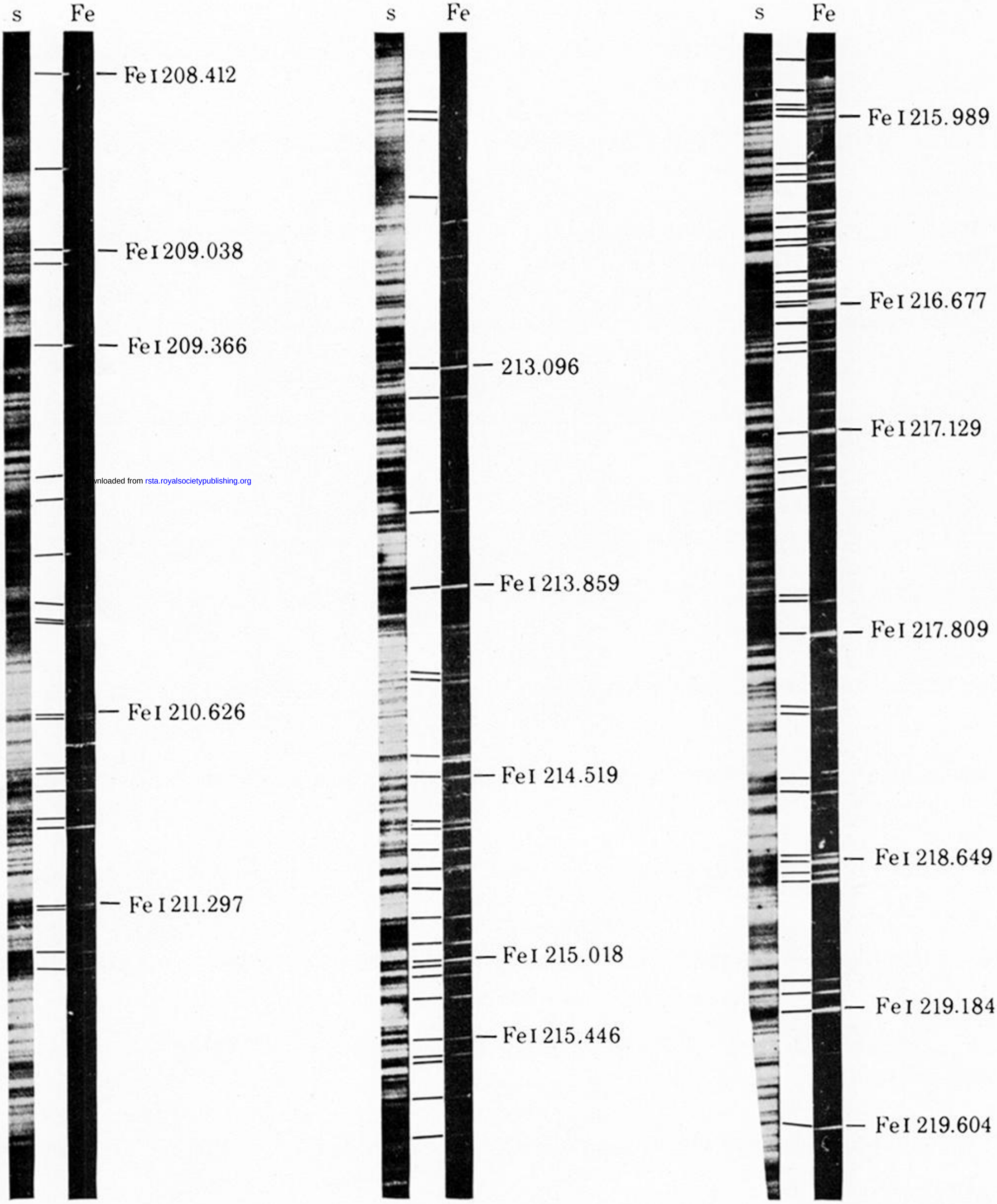

FIGURE 3. Comparison of (s) solar spectrum with (Fe) laboratory Fe source over range 208 to 220 nm using the same instrument. Successive echelle cycles have been joined together.